Curr Cardiovasc Imaging Rep (2016) 9: 8
DOI 10.1007/s12410-016-9370-4

Cardiac CT Scanner Technology: What Is New and What Is Next?

Sandra S. Halliburton[1] · **Prabhakar Rajiah**[2]

Published online: 3 February 2016
© Springer Science+Business Media New York 2016

Abstract Technical specifications for multi-detector row computed tomography (CT) scanners from different manufacturers were very similar until the introduction of 64-slice scanners but then began to diverge with fundamental differences in the number of X-ray sources, detector geometry, gantry rotation time, and reconstruction algorithms. These hardware and software advancements were largely driven by clinical requirements for cardiac CT. This article provides an overview of technologies available on state-of-the-art CT systems and the clinical needs they seek to address.

Keywords Dual energy · Iterative reconstruction · Detectors

Introduction

CT hardware and software advancements during the last two decades have largely been driven by clinical requirements for cardiac CT including high temporal resolution to minimize the effects of cardiac motion, high spatial resolution to assess small structures like the coronary arteries, wide coverage in the z-direction (direction of table movement) per rotation to shorten scan times, optimization of X-ray spectra to discriminate tissues (e.g., plaque components, normal and infarcted myocardium), and low radiation dose to minimize patient risk. Critical specifications for state-of-the-art CT scanners from the major manufacturers are listed in Table 1.

The primary approach to improving temporal resolution pursued by all manufacturers has been to decrease gantry rotation time. The temporal resolution, or time required to obtain the data for a single image, is estimated as one half of the gantry rotation time. The fastest commercially available gantry rotates 360° in 250 ms with most state-of-the-art CT systems capable of rotation times equal to or less than 280 ms. One manufacturer also developed a specialized scanner type, a dual-source CT scanner, with two X-ray tube/detector systems that rotate together to further reduce the temporal resolution to one fourth of the gantry rotation time.

A major determinant of z- or through-plane spatial resolution, the width of the active element of a single detector, has remained unchanged at 0.5–0.6 mm for years [1]. However, other advancements like deflection of the X-ray focal spot between 2 z-positions (ie, z-flying focal spot) to acquire 2 overlapping slices for each detector row have enabled improved spatial resolution. Other improvements to detectors and detector electronics have recently been introduced that enable improved spatial resolution. These will be discussed in detail below. The highest through-plane spatial resolution of current MDCT scanners has been reported to be around 0.3 mm and in-plane spatial resolution in the range of 0.23 mm to 0.4 mm.

Z-coverage per rotation is increased by increasing the number of detector rows mounted on the gantry opposite the X-ray tube (s). Currently, two commercially available CT scanners permit coverage of 160 mm in a single rotation with other state-of-the-art systems providing either 40 or 80 mm of coverage in the z-direction. Wider z-coverage permits acquisition

This article is part of the Topical Collection on *Cardiac Computed Tomography*

✉ Sandra S. Halliburton
Sandra.halliburton@philips.com

[1] Philips Healthcare, 595 Miner Road, Highland Heights, OH 44143, USA

[2] Cardiothoracic Imaging Section, Radiology, University Hospitals of Cleveland Case Medical Center, Cleveland, OH, USA

Table 1 Critical specifications for state-of-the-art CT scanners from the major manufacturers

Scanner	Collimated detector row width (mm)	Number of Detector rows	Coverage (mm/rot)	Rotation time (ms)	Temporal resolution (ms)
GE Revolution	0.625	256	160	280	140
Hitachi SCENARIA	0.6	64	38.4	350	175
Philips Brilliance iCT	0.625	128	80	270	135
Samsung NExCT 7	0.625	128	80	250	125
Siemens FORCE	0.6	96	57.6	250	66
Toshiba AquilionONE	0.5	320	160	275	137.5

of cardiac data in fewer heart beats, minimizing the opportunity for misregistration between slices and maximizing the probability of consistent depiction of contrast agent flow through the region-of-interest (critical for myocardial perfusion studies).

Recent areas of advancement that will be discussed in detail have focused on optimization of the X-ray spectra to improve tissue discrimination, improvements in detectors and detector electronics to improve spatial resolution and increase dose efficiency, and development of innovative image reconstruction algorithms to improve spatial resolution and reduce needed dose per scan.

Optimal X-ray Spectra

In diagnostic CT, X-rays are produced at multiple energies with the highest energy (and the range of energies) controlled by selection of the peak tube potential applied across the X-ray tube. The specific energy of each photon in the X-ray spectra determines the dominant mechanisms of its interaction with tissue and, subsequently, its attenuation. The result is energy-dependent X-ray attenuation. CT scanners typically produce a single polychromatic or polyenergetic X-ray beam and record the attenuated X-rays using energy-integrating solid-state detectors. The resulting attenuation data is characteristic of X-rays with energy equal to the average energy of the X-ray spectra.

Expanded Energy Range

Until recently, the lowest peak tube potential available on diagnostic CT scanners was 80 kVp. A 70-kVp setting has been made available on some scanners. Lower tube potentials offer the advantage of improved image contrast because of an increase in the probability of photoelectric interactions between incident X-ray photons and target tissue at lower X-ray energies. The limitation at 70 kVp for standard diagnostic CT is image noise because of lower X-ray penetrability.

The use of 70 kVp is indicated for cardiac imaging of pediatric patients and smaller adults. One group compared 80- and 70-kVp settings in phantoms and children with congenital heart disease and concluded 70-kVp imaging may be appropriate despite higher noise because of the increase in contrast-to-noise ratio (CNR) [2]. Meyer et al. demonstrated the equivalency of coronary artery image quality for adults with a BMI less than 26 kg/m^2 scanned at 70 kVp and overweight adults (BMI = 26–30 kg/m^2) scanned at 100 kVp [3].

Dual Energy CT

Dual energy CT refers to the acquisition of two spectrally distinct attenuation data sets from the same anatomical region of interest. Differences in X-ray attenuation at high versus low energies can improve tissue discrimination. The signal from very dense tissues like iodine and calcium changes the most between high and low X-ray spectra while the signal from less dense tissues like fat and blood changes the least.

Current strategies for acquiring dual-energy data include using specialized scanners with either two X-ray tube/detector systems, a single X-ray tube/detector system capable of rapid tube potential switching, a single X-ray tube with a filter for splitting the X-ray beam, a single X-ray tube and dual layers of energy-sensitive detectors, or a single X-ray tube with a wide detector array.

Dual-Source CT Two X-ray tubes are operated simultaneously but at different peak tube potentials (e.g., tube A is operated at 140 kVp and tube B at 80 kVp). Data are simultaneously recorded by each tube's corresponding detector system. Two complete data sets, a high-energy data set and a low-energy data set, are then available for each spatial location [4].

Alternating Tube Potential A single X-ray tube alternates the peak potential applied across the tube from 80 to

140 kVp every 0.2 ms for successive X-ray projections as the X-ray tube and its detector system are rotated around the patient. Two interleaved but complete data sets are then available for each spatial location [5].

Split-Beam Technology A single X-ray tube is operated at a single tube potential of 120 kVp but the resulting X-ray spectrum is filtered before reaching the patient using tin (Sn) and gold (Au) to create high- and low-energy spectra, respectively. Data from both spectra are simultaneously recorded by different rows of the detector array until the desired anatomy is covered. Two complete data sets, a high (Sn) and low (Au) energy data set, are then available for each spatial location.

Dual Layer Detector A single X-ray tube is operated at a single tube potential (e.g., 120 kVp) and two layers of detectors are used to acquire both low-energy and high-energy X-ray photons simultaneously [6]. The low-energy photons are captured by the upper layer while the high-energy photons penetrate this layer and are collected by the bottom layer. Two complete data sets acquired simultaneously are then available for each spatial location.

Consecutive Rotations with Wide Detector Array A single X-ray tube is rotated twice around the same anatomic region at different peak potentials (80, 135 kVp) [7]. A complete data set is acquired during each rotation, one at a lower energy and one at higher energy resulting in two data sets for each spatial location.

Dual energy data sets obtained using any of the technologies described above can be displayed individually as conventional single-energy images (e.g., 80 kVp or 140 kVp images), as combined or mixed images (e.g., 120 kVp or 120 kVp equivalent images), as virtual monoenergetic images, as material composition images, or as effective atomic number images [8].

Mixed Images (aka, Combined, Average Weighted) Images Images created with variable contributions from low- and high-energy data to yield images with similar attenuation properties to conventional single-energy images.

Virtual Monoenergetic Images Images generated from dual-energy data to display tissue attenuation properties similar to those that would result from imaging with a monoenergetic beam at a single kiloelectron voltage (keV) level (Fig. 1). Reconstruction of images at higher monoenergies enables greater levels of artifact reduction, such as metal and beam hardening artifacts.

Material Images Images with selected materials, identified using dual energy data, either displayed or removed. The tissue within a voxel can be decomposed into selected materials (eg, iodine and water) with known attenuation properties at high and low X-ray energies. The identification of iodine, for example, allows generation of a blood pool image displaying only iodine. The resulting iodine maps can be depicted as grayscale images or superimposed as a color overlay on attenuation images. Alternatively, the identification of iodine allows creation of images displaying no iodine and mimicking non-contrast images. The resulting images are called virtual non-contrast images.

Effective Atomic Number ($Z_{effective}$) Images Images displaying pixel values equal to the $Z_{effective}$ of the tissue contained within each corresponding patient voxel. Material decomposition of tissues using high and low-energy spectra permits characterization of tissues based on $Z_{effective}$. $Z_{effective}$ maps can be displayed as grayscale images or overlayed as color on attenuation images.

DECT has proven useful for several cardiovascular indications [8]. The conspicuity of myocardial perfusion defects is improved on DECT-derived iodine-maps compared to single-energy CT images which facilitates the identification of hemodynamically significant coronary lesions [9]. DECT iodine-maps have been shown to improve detection of scar on delayed-enhancement images, with no difference in diagnostic accuracy compared to MRI (90 % in both) [10]. With DECT, maps displaying iodine with units of concentration (mg/ml) can also be created that permit quantification of myocardial iodine making the discrimination between healthy and ischemic or necrotic tissue less subjective [11•]. Virtual monoenergetic images are also useful for detecting myocardial perfusion defects as they are associated with fewer beam hardening artifacts and reduced false positive rates. Several studies have shown high sensitivity, specificity, and accuracy for detecting perfusion defects from dual energy CT compared to magnetic resonance imaging (MRI) or single-photon emission computed tomography (SPECT) [4, 9, 12–15].

DECT-derived images have potential for improved coronary plaque characterization, particularly in distinguishing between calcific and noncalcific components [16]. Calcium can also be separated from iodine using dual energy data. This permits generation of virtual non-contrast images and determination of a calcium score from a contrast-enhanced scan; good correlation

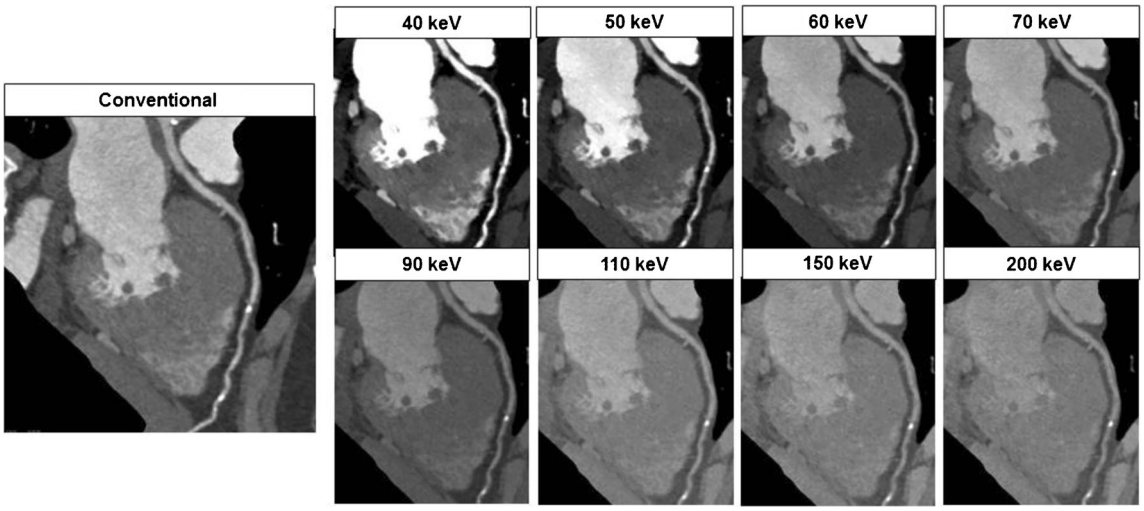

Fig. 1 Conventional 120 kVp and virtual monoenergetic coronary CT angiograms displaying the left anterior descending artery. Lower energy virtual monoenergetic images are useful for enhancing the iodine signal within vascular structures. Higher energy virtual monoenergetic images are useful for visualizing coronary artery calcium. Note the similarity of the conventional 120 kVp image and the 70 keV image (120 kVp monoequivalent for this scanner)

has been shown between calcium volumes obtained from virtual and true non-contrast images [17, 18]. Other potential advancements in coronary imaging compared to single-energy CT include better visualization of coronary lumen in the presence of calcified plaque [19] and better evaluation of coronary stent patency [20, 21].

The availability of dual energy data also offers the potential for detecting and quantifying certain elements present in the organs and tissues and introducing new cardiac CT applications. For example, dual energy CT has been used to detect and quantify myocardial iron [22].

With DECT, there are opportunities for lowering both radiation and contrast dose. The availability of virtual non-contrast scans can obviate the need for a non-contrast acquisition in multi-phasic studies, thereby minimizing radiation dose [23–28]. Lower volumes of iodinated contrast material are necessary for angiographic studies due to the ability to boost vascular signal in monoenergetic images at lower energies [29, 30••, 31].

Spectral CT

Spectral CT utilizes multiple (more than two) spectrally distinct attenuation datasets obtained at different photon energies to distinguish tissues and materials. Photon counting CT is currently the closest implementation to a full spectral imaging solution. Photon counting CT uses semiconductor detectors such as calcium zinc telluride (CZT) or cadmium telluride (CdTe) to separate incident X-ray photons into “energy bins”. Creation of narrow energy bins over the range of the generated X-ray spectrum may permit accurate classification of material, even at low material concentrations [32]. Technical barriers to clinical implementation include the slow response of the detector system which necessitates slow rotation speeds and long examination times.

Improved Detectors/Detector Electronics

The same basic detector technology has been used in commercial CT scanners for the last three decades [33]. The standard detector element is a solid-state detector composed of scintillator material coupled to a photodiode. Scintillators are individually cut and polished and coated with reflectors to prevent cross-talk (leakage of generated signal) between detector elements. The scintillator material converts x-rays into visible light and the light is detected by a photodiode. The photodiode converts visible light into an electrical signal that is transmitted to a computer. Detectors are typically built in a discrete circuit such that diodes send out analog signals to an analog-to-digital converter circuit board, then digital signals are sent to a separate digital circuit board.

Garnet-Based Scintillator Material

The decay rate of scintillator material, or how fast scintillator molecules emit light and return to a ground state after being promoted to high-energy states by X-rays, largely determines the response time of a detector. New materials with shorter decay times have been introduced that have enabled faster response times. Faster detector response times offer advantages including the capacity to support increased data sampling per rotation without a time penalty yielding improved x–y (in-plane) spatial resolution.

Improved spatial resolution achieved in part with updated scintillator material provided more accurate measurement of in-stent diameter in a coronary stent phantom [34]. The same technology demonstrated better image quality and measurement accuracy in vivo for coronary stents with diameters ranging from 2.75 to 3.5 mm [35, 36].

Integrated Detector Electronics

The distance between the photodiode and the electronics in a detector is a source of noise. Fully integrated circuit detectors have recently been introduced that combine photodiodes and electronics into a single unit to decrease the distance between the two components. This reduces the path of the analog signal and reduces noise and cross-talk between adjacent detector elements.

A positive consequence of reduced noise and better defined individual slice profiles as a result of reduced cross-talk between detector rows is improved z-resolution and the potential to reconstruct thinner slices with sufficient signal for routine clinical use. Improved spatial resolution with integrated circuit detectors was shown to improve coronary CT image quality and in-stent stenosis quantification compared to a conventional detector in several phantom studies [37, 38]. Alternatively, reduced electronic noise with integrated circuit detectors can be exploited to lower dose while maintaining image quality as demonstrated for routine chest examinations [39].

Image Reconstruction

Non-linear iterative reconstruction (IR) algorithms are gradually replacing traditional, linear filtered back projection (FBP) algorithms as the standard approach to CT image reconstruction. Most currently available IR algorithms only model photon counting statistics or noise to increase dose efficiency and reduce noise and noise-related artifacts [40–44]. Some IR algorithms employ models of the scanner geometry and the interaction of x-rays with the imaged objects as well as statistical noise models. These so-called model-based [45] or knowledge-based [46] IR algorithms are the most computationally intensive but offer the greatest potential for reduction of noise and other artifacts and improvement in spatial resolution compared to FBP [47].

IR algorithms are primarily aimed at reducing dose without a loss in image quality for particular clinical applications. This is challenging because traditional CT image quality metrics do not hold for non-linear reconstruction algorithms. For example, spatial resolution is independent of contrast and noise levels with linear reconstruction but dependent on contrast and noise with non-linear reconstruction.

The Food and Drug Administration has demanded utilization of novel image quality tools to assess dose reduction claims with newly introduced IR algorithms. These tools are task-based and focus on objective assessment of low contrast detectability (the ability to discriminate a low contrast object from its surroundings). Typically, a phantom-based task (e.g., identifying the presence or absence of a signal in a given image) is defined and performed by a human observer or a computational model observer. A figure of merit (e.g., receiver operator characteristic [ROC] curve, detectability index) assessing observer performance on the task is then obtained providing an objective measure of image quality.

Although meaningful, these studies stop short of ensuring no diagnostic information is lost at lowered doses for a specific clinical task which necessitates clinical validation studies. A prospective, multicenter, multivendor noninferiority trial assessed the potential for IR to enable reduced radiation exposure during coronary CT angiography compared to image reconstruction with FBP [48]. Results demonstrated that image quality was maintained with the combined use of 30 % reduced tube currents and IR algorithms when compared with the delivery of standard tube currents and reconstruction with FBP (Table 2).

Several clinical studies have assessed the diagnostic accuracy of coronary CT angiograms acquired at lowered doses and reconstructed with novel IR algorithms using invasive coronary angiography (ICA) as a standard of reference [44, 49••, 50, 51]. Outcomes included diagnostic accuracy, sensitivity, specificity, negative predictive value and positive

Table 2 Results from the Protection V study comparing images reconstructed with iterative reconstruction techniques from data acquired with 30 % reduced tube currents to images reconstructed with filtered back projection from data acquired with standard tube currents. Reprinted with permission from [48]

	Reduced current + IR	Standard currect + FBP	*p* value
Image quality score	3.5 (3.0–4.0)	3.4 (2.8–4.0)	0.19
GE	3.3 (2.8–3.8)	3.5 (2.8–4.0)	*
Philips	3.3 (2.8–4.0)	3.3 (2.5–3.8)	*
Siemens	4.0 (3.5–4.0)	3.5 (3.0–4.0)	*
Toshiba	3.5 (2.9–4.0)	3.3 (2.8–4.0)	*
Vessel contour blurring score	3.0 ± 0.9	3.1 ± 0.9	0.27
Patients with stenosis >50 %	44 (21.8)	41 (20.7)	0.79
Signal intensity, HU	494 ± 149	488 ± 145	0.66
Image noise, HU	28.7 ± 8.2	30.9 ± 12.1	0.04
Signal/noise ratio	18.7 ± 8.2	17.6 ± 7.4	0.16
Contrast/noise ratio	15.0 ± 7.4	14.0 ± 6.6	0.16
Dose-length-product, mGy cm	157 (114–239)	222 (141–319)	<0.0001
GE	126 (100–252)	138 (132–265)	*
Philips	142 (103–178)	181 (139–244)	*
Siemens	230 (134–293)	319 (198–412)	*
Toshiba	159 (120–183)	237 (207–316)	*
Effective does estimate, mSv	2.2 (1.6–3.3)	3.1 (2.0–4.5)	<0.0001
Need for additional clinical testing	15 (7.7)	15 (7.9)	0.94

Values are median (interquartile range), mean ± SD, or *n* (%)

FBP filtered back projection, *IR* iterative image reconstruction

*No testing for statistical significance was performed because the study was not powered for intravendor or intervendor comparisons

predictive value. Several studies found comparable or improved image quality at lower doses with IR compared to higher doses with standard (e.g., FBP) algorithms and comparable outcomes [44, 50, 51]. One study, evaluating only lower dose IR in comparison to ICA, noted significant differences in specificity, PPV, and accuracy between patients with calcium scores greater than 400 and calcium scores less than 400 (92.1 versus 97.9 %, 76.0 versus 86.7 % and 91.7 versus 96.6 %) indicating limitations exist using CT for the assessment of coronary stenosis in patients with a high calcium burden even using advanced reconstruction techniques [49••].

It is important to note that specific algorithms differ widely across manufacturers as do different algorithms from the same manufacturer. The resulting noise patterns and artifacts in reconstructed images differ and conclusions based on evaluation of one algorithm are not always transferable to other algorithms.

Future

Future CT hardware and software advancements will likely continue to be driven by the clinical requirements for cardiac CT: high temporal resolution, high spatial resolution, and soft tissue discrimination. Therefore, increases in gantry rotation speed, decreases in the width of detector elements, increases in dose efficiency of detectors, availability of energy discriminating detectors and improvements in iterative reconstruction techniques can be expected. Continued divergence of system designs across vendors is likely because optimization of multiple features simultaneously is hindered by currently required tradeoffs in performance, as well as cost.

Conclusion

Continuous technical innovations have enabled gantry rotation times as low as 250 ms with resulting temporal resolutions as low as approximately 70 ms. The number of detector rows on these systems range from 64 to 320 covering anywhere from approximately 40 to 160 mm of anatomy. Improvements in detector response time and the combination of electronics and photodiodes into a single, fully integrated circuit has contributed to improvements in spatial resolution to as low as 0.23 mm in-plane and 0.3 mm through-plane. Nonlinear reconstruction algorithms, particularly model-based iterative reconstruction techniques, are increasingly available and permit significant dose reduction compared to standard linear reconstruction algorithms.

Optimization of X-ray spectra including expansion of the minimum peak tube potential to 70 kVp and the availability of

multiple solutions for obtaining data from the same anatomic region at two peak tube potentials (dual energy) show promise for improving tissue discrimination. These advances continue to extend the clinical utility of CT for cardiovascular indications.

Compliance with Ethical Standards

Conflict of Interest Dr. Rajiah reports he has received speaker fees from Philips Healthcare during the writing of this paper. Dr. Halliburton reports she is a full-time employee of Philips Healthcare.

Human and Animal Rights and Informed Consent This article does not contain any studies with human or animal subjects performed by any of the authors.

References

Papers of particular interest, published recently, have been highlighted as:
- • Of importance
- •• Of major importance

1. Halliburton S, Dey D, Einstein A, et al. State-of-the-art in CT Hardware and Scan Modes for Cardiovascular CT. J Cardiovasc Comput Tomogr. 2012;6:154–63.
2. Durand S, Paul JF. Comparison of image quality between 70 kVp and 80 kVp: application to paediatric cardiac CT. Eur Radiol. 2014;24(12):3003–9.
3. Meyer M, Haubenreisser H, Schoepf UJ, et al. Closing in on the K edge: coronary CT angiography at 100, 80, and 70 kV-initial comparison of a second- versus a third-generation dual-source CT system. Radiology. 2014;273(2):373–82.
4. Kang DK, Schoepf UJ, Bastarrika G, Nance Jr JW, Abro JA, Ruzsics B. Dual-energy computed tomography for integrative imaging of coronary artery disease: principles and clinical applications. Semin Ultrasound CT MR. 2010;31:276–91.
5. So A, Lee TY, Imal Y, et al. Quantitative myocardial perfusion imaging using rapid kVp switch dual energy CT: a preliminary experience. J Cardiovasc Comput Tomogr. 2011;5(6):430–2.
6. Roessl E, Herrmann C, Kraft E, Proksa R. A comparative study of a dual-energy-like imaging technique based on counting-integrating readout. Med Phys. 2011;38:6416.
7. So A, Hsieh J, Narayanan S, et al. Dual-energy CT and its potential use for quantitative myocardial CT perfusion. J Cardiovasc Comput Tomogr. 2012;6:308–17.
8. Rajiah P, Halliburton SS. Dual energy imaging in cardiovascular CT: current status and impact on radiation, contrast and accuracy. Curr Cardiovasc Imaging Rep. 2014;7:9289.
9. Arnoldi E, Lee YS, Ruzsics B, et al. CT detection of myocardial blood volume deficits: dual-energy CT compared with single-energy CT spectra. J Cardiovasc Comput Tomogr. 2011;5:421–9.
10. Bauer RW, Kerl JM, Fischer N, et al. Dual-energy CT for the assessment of chronic myocardial infarction in patients with chronic coronary artery disease: comparison with 3T MRI. Am J Roentgenol. 2010;195:639–46.
11. • Sánchez-Gracián DC, Pernas RO, López CT, et al. Quantitative myocardial perfusion with stress dual-energy CT: iodine concentration differences between normal and ischemic or necrotic myocardium. Initial experience. Eur Radiol. 2015; 1–9. **This study demonstrates the ability to not only identify iodine but also quantify its concentration using dual energy CT. This may reduce interobserver variability in the discrimination of normal and diseased myocardium with CT and improve the accuracy compared to single energy CT.**
12. Kim SM, Chang SA, Shin W, Choe YH. Dual-energy CT perfusion during pharmacologic stress for the assessment of myocardial perfusion defects using a second-generation dual-source CT: a comparison with cardiac magnetic resonance imaging. J Comput Assist Tomogr. 2014;38:44–52.
13. Weininger M, Schoepf UJ, Ramachandra A, et al. Adenosine-stress dynamic real-time myocardial perfusion CT and adenosine-stress first-pass dual-energy myocardial perfusion CT for the assessment of acute chest pain: initial results. Eur J Radiol. 2012;81:3703–10.
14. Meinel FG, De Cecco CN, Schoepf UJ, et al. First-arterial-pass dual-energy CT for assessment of myocardial blood supply: do we need rest, stress, and delayed acquisition? comparison with SPECT. Radiology. 2014;270:708–16.
15. Ruzsics B, Lee H, Zwerner PL, Gebregziabher M, Costello P, Schoepf UJ. Dual-energy CT of the heart for diagnosing coronary artery stenosis and myocardial ischemia-initial experience. Eur Radiol. 2008;18:2414–24.
16. Barreto M, Schoenhagen P, Nair A, et al. Potential of dual-energy computed tomography to characterize atherosclerotic plaque: ex vivo assessment of human coronary arteries in comparison to histology. J Cardiovasc Comput Tomogr. 2008;2:234–42.
17. Schwarz F, Nance Jr JW, Ruzsics B, Bastarrika G, Sterzik A, Schoepf UJ. Quantification of coronary artery calcium on the basis of dual-energy coronary CT angiography. Radiology. 2012;264: 700–7.
18. Yamark D, Pavlicek W, Boltz T, Panse PM, Akay M. Coronary calcium quantification using contrast-enhanced dual-energy computed tomographic scans. J Appl Clin Med Phys. 2013;14:4014.
19. Boll DT, Merkle EM, Paulson EK, Mirza RA, Fleiter TR. Calcified vascular plaque specimens: assessment with cardiac dual-energy multi detector CT in anthrophomorphically moving heart phantom. Radiology. 2008;249:119–26.
20. Boll DT, Merkle EM, Paulson EK, Fleiter TR. Coronary stent patency: dual-energy multidetector CT assessment in a pilot study with anthropomorphic phantom. Radiology. 2008;247:687–95.
21. Secchi F, De Cecco CN, Spearman JV, et al. Monoenergetic extrapolation of cardiac dual energy CT for artifact reduction. Acta Radiol. 2015;56(4):413–8.
22. Hazirolan T, Akpinar B, Unal S, Gumruk F, Haliloglu M, Alibek S. Value of dual energy computed tomography for detection of myocardial iron deposition in thalassaemia patients: initial experience. Eur J Radiol. 2008;68:442–5.
23. Numburi UD, Schoenhagen P, Flamm SD, et al. Feasibility of dual-energy CT in the arterial phase: imaging after endovascular aortic repair. Am J Roentgenol. 2010;195:486–93.
24. Chandarana H, Godoy MC, Vlahos I, et al. Abdominal aorta: evaluation with dual-source dual-energy multidetector CT after endovascular repair of aneurysms—initial observations. Radiology. 2008;249:692–700.
25. Sommer WH, Graser A, Becker CR, et al. Image quality of virtual noncontrast images derived from dual-energy CT angiography after endovascular aneurysm repair. J Vasc Interv Radiol. 2010;21:315–21.
26. Stolzmann P, Frauenfelder T, Pfammatter T, et al. Endoleaks after endovascular abdominal aortic aneurysm repair: detection with dual-energy dual-source CT. Radiology. 2008;249:682–91.
27. Maturen KE, Kleaveland PA, Kaza RK, et al. Aortic endograft surveillance: use of fast-switch kVp dual-energy computed

tomography with virtual noncontrast imaging. J Comput Assist Tomogr. 2011;35:742–6.
28. Shaida N, Bowden DJ, Barrett T, et al. Acceptability of virtual unenhanced CT of the aorta as a replacement for the conventional unenhanced phase. Clin Radiol. 2012;67:461–7.
29. Schenzle JC, Sommer WH, Neumaier K, et al. Dual energy CT of the chest: how about the dose? Investig Radiol. 2010;45:347–53.
30.•• Dubourg B, Caudron J, Lestrat JP, Bubenheim M, Lefebvre V, Godin M, et al. Single-source dual-energy CT angiography with reduced iodine load in patients referred for aortoiliofemoral evaluation before transcatheter aortic valve implantation: impact on image quality and radiation dose. Eur Radiol. 2014;24(11):2659–68. **This study demonstrates CT images of sufficient quality for aortoiliofemoral evaluation before transcatheter aortic valve implantation (TAVI), a rapidly growing indication for cardiovascular CT, can be obtained with a 50% reduction in iodine load if dual energy, rather than single energy, techniques are used to acquire data.Low-contrast dose is preferred in many TAVI patients with severe renal dysfunction, in whom the intravenous administration of iodinated contrast can result in kidney damage**.
31. Carrascosa P, Leipsic JA, Capunay C, et al. Monochromatic image reconstruction by dual energy imaging allows half iodine load computed tomography coronary angiography. Eur J Radiol. 2015;84(10):1915–20.
32. Roessl E, Proksa R. K-edge imaging in x-ray computed tomography using multi-bin photon counting detectors. Phys Med Biol. 2007;52(15):4679–96.
33. Pelc N. Ann Biomed Eng. 2014;42(2):260–8.
34. Tanami Y, Jinzaki M, Yamada M, Imai Y, Seqawa K, Kuribayashi S. Improvement on in-stent lumen measurement accuracy with new high-definition CT in a phantom model: comparison with conventional 64-detector row CT. Int J Cardiovasc Imaging. 2012;28(2):337–42.
35. Yang WJ, Zhang H, Li JY, et al. High-definition computed tomography for coronary artery stents imaging compared with standard-definition 64-row multidetector computed tomography: an initial in vivo study. J Comput Assist Tomogr. 2012;36(3):295–300.
36. Fuchs TA, Stehli J, Fietchter M, et al. First in vivo head-to-head comparison of high-definition versus standard-definition stent imaging with 64 slice computed tomography. Int J Cardiovasc Imaging. 2013;29:1409–16.
37. von Spiczak J, Morsback F, Winklhofer S, et al. Coronary artery stent imaging with CT using an integrated electronics detector and iterative reconstructions: first in vitro experience. J Cardiovasc Comput Tomogr. 2013;7(4):215–22.
38. Morsbach F, Desbiolles L, Plass A, et al. Stenosis quantification in coronary CT angiography: impact of an integrated circuit detector with iterative reconstruction. Investig Radiol. 2013;48:32–40.
39. Ebner L, Knobloch F, Huber A, et al. Feasible dose reduction in routine chest computed tomography maintaining constant image quality using the last three scanner generations: from filtered back projection to sinogram-affirmed iterative reconstruction and impact of the novel fully integrated detector design minimizing electronic noise. Clin Imaging Sci. 2014;4:38.
40. Renker M, Ramachandra A, Schoepf JU, et al. Iterative image reconstruction techniques: applications for cardiac CT. J Cardiovasc Comput Tomogr. 2011;5:225–30.
41. Tomizawa N, Nojo T, Akahane M, et al. Adaptive iterative dose reduction in coronary CT angiography using 320 row CT: assessment of radiation dose reduction and image quality. J Cardiovasc Comput Tomogr. 2012;6:318–24.
42. Hou Y, Xu S, Guo W, et al. The optimal dose reduction level using iterative reconstruction with prospective ECG-triggered coronary CTA using 256-slice MDCT. Eur J Radiol. 2012;81(12):3905–11.
43. Leipsic J, Labounty TM, Min JK, et al. Estimated radiation dose reduction using adaptive statistical iterative reconstruction in coronary CT angiography: the ERASIR study. Am J Roentgenol. 2010;195:655–60.
44. Layritz C, Schmid J, Achenbach S, et al. Accuracy of prospectively ECG-triggered very low-dose coronary dual-source CT angiography using iterative reconstruction for the detection of coronary artery stenosis: comparison with invasive catheterization. Eur Heart J Cardiovasc Imaging. 2014;15(11):1238–45.
45. Stehli J, Fuchs TA, Bull S, et al. Accuracy of coronary CT angiography using a submillisevert fraction of radiation exposure. J Am Coll Cardiol. 2014;64:772–80.
46. Halpern EJ, Gingold EL, White H, et al. Evaluation of coronary artery image quality with knowledge based iterative model reconstruction. Acad Radiol. 2014;21:805–11.
47. Nelson RC, Feuerlein S, Boll DT. New iterative reconstruction techniques for cardiovascular computed tomography: how do they work, and what are the advantages and disadvantages? J Cardiovasc Comput Tomogr. 2011;5:286–92.
48. Deseive S, Chen M, Korosoglou G, et al. Prospective randomized trial on radiation dose estimates of CT angiography applying iterative image reconstruction. The protection V study. J Am Coll Cardiol Img. 2015;8(8):888–96.
49.•• Hou J, Ma Y, Fan W. Diagnostic accuracy of low-dose 256-slice multi-detector coronary CT angiography using iterative reconstruction in patients with suspected coronary artery disease. Eur Radiol. 2014;24:3–11. **This clinical validation study evaluates images reconstructed from low dose data using an iterative reconstruction technique. These low dose images demonstrate satisfactory image quality and high diagnostic accuracy for the evaluation of coronary artery disease in comparison to invasive coronary angiography. The study also highlights, however, that even this advanced reconstruction technique is limited in the assessment of coronary stenosis in patients with a high calcium burden**.
50. Yin WH, Lu B, Li N, et al. Iterative reconstruction to preserve image quality and diagnostic accuracy at reduced radiation dose in coronary CT angiography: an intraindividual comparison. JAm Coll Cardiol Img. 2013;6(12):1239–49.
51. Pontone G, Andreini D, Bartorelli AL. Feasibility and diagnostic accuracy of a low radiation exposure protocol for prospective ECG-triggering coronary MDCT angiography. Clin Radiol. 2012;67:207–15.